

Article

Integrated Imaging and Spectroscopic Analysis of Painted Fresco Surfaces Using Terahertz Time-Domain Technique

Alessia Artesani ^{1,*}, Francesco Abate ^{2,3}, Raffaella Lamuraglia ^{2,3}, Maria Antonietta Baldo ³,
Federica Menegazzo ^{2,3} and Arianna Traviglia ²

¹ Department of Biomedical Sciences, Humanitas University, 20090 Milan, Italy

² Center for Cultural Heritage Technology, Istituto Italiano di Tecnologia, 30172 Venice, Italy; francesco.abate@iit.it (F.A.); raffaella.lamuraglia@iit.it (R.L.); fmenegaz@unive.it (F.M.); arianna.traviglia@iit.it (A.T.)

³ Department of Molecular Sciences and Nanosystems, Università Ca' Foscari Venezia, 30172 Venice, Italy; toni@unive.it

* Correspondence: alessia.artesani@hunimed.eu

Abstract: Terahertz time-domain (THz-TD) imaging plays an increasingly significant role in the study of solid-state materials by enabling the simultaneous extraction of spectroscopic composition and surface topography in the far-infrared region (3–300 cm⁻¹). However, when applied to works of art in reflection configuration, significant challenges arise, including weak signal intensity, multiple signal losses, and surface distortion. This study proposes a practical solution to overcome these limitations and conducts an integrated imaging and spectroscopic analysis on painted fresco surfaces, allowing for the retrieval of surface thicknesses, material distribution, and pigment spectroscopic signals. The study addresses the issue of surface geometrical distortion, which hampers the accurate determination of the THz phase signal. By tackling this challenge, this work successfully determines the absorption coefficient for each point on the surface and retrieves spectroscopic signatures. Additionally, the temporal deconvolution technique is employed to separate different layers of the sample and differentiate between outer and inner surface topography. The objective of this study is to demonstrate the advantages and limitations of THz-TD imaging in determining surface thicknesses, material distribution, and pigment spectroscopic signals. The results obtained highlight the potential of THz-TD imaging in investigating painted works of art, offering new possibilities for routine analysis in the field of cultural heritage preservation.

Keywords: terahertz time domain; spectroscopy; frescos



Citation: Artesani, A.; Abate, F.; Lamuraglia, R.; Baldo, M.A.; Menegazzo, F.; Traviglia, A. Integrated Imaging and Spectroscopic Analysis of Painted Fresco Surfaces Using Terahertz Time-Domain Technique. *Heritage* **2023**, *6*, 5202–5212. <https://doi.org/10.3390/heritage6070276>

Academic Editors: Corinna Ludovica Koch Dandolo and Jean-Paul Guillet

Received: 30 May 2023

Revised: 6 July 2023

Accepted: 7 July 2023

Published: 10 July 2023



Copyright: © 2023 by the authors. Licensee MDPI, Basel, Switzerland. This article is an open access article distributed under the terms and conditions of the Creative Commons Attribution (CC BY) license (<https://creativecommons.org/licenses/by/4.0/>).

1. Introduction

Terahertz (THz) radiation refers to the range of frequencies in the far-infrared region between 3 and 300 cm⁻¹, or, in terms of wavelength, between 3 mm and 30 μm [1]. In heritage material studies, this radiation is particularly appreciated for providing a safe and non-invasive method for analyzing objects without posing long-term risks to their chemical stability. In fact, it is non-ionizing and can penetrate many materials that are opaque in the visible and near-infrared frequencies [2–4]. When employed with imaging or tomography devices, THz time domain (THz-TD) can enable the investigation of the internal structure of objects and provide information related to their conservation conditions in a completely non-invasive manner [1,5,6].

To the best of our knowledge, and as already reported in a recent paper by Piccolo and co-authors [7], the THz-TD technique has been largely employed to investigate virtual cross-sections and discriminate details such as paint stratigraphy; however, it has never been used in combination with spectroscopy mapping. This work proposes, for the first time, the application of a combined strategy to treat THz-TD image data and retrieve

spectral characterization on a real artwork surface, facing the limitations imposed by the technique and inherited by the broad-band spectroscopic approach.

A significant advantage of employing THz radiation is, in fact, the utilization of a broad-band source and simple acquisition procedures for spectroscopic analysis. The characterization of spectra at far-infrared frequencies can yield more specific absorption peaks than those gathered in the mid- and near-infrared regions, as THz waves excite the vibrational modes of molecules and crystalline lattices [2,8–11]. THz-TD spectroscopy provides both signal amplitude and phase spectral information, the former being linked to material absorption, and the latter related to sample thicknesses and density. The complementary determination of these two components of the signal can further enable the direct measurement of the material refractive index.

However, some constraints might limit the method and reduce the technique's performance. Firstly, the signal-to-noise ratio is one of the primary drawbacks of THz-based technologies, because THz radiation has a high penetration power, and material scattering can significantly reduce the signal [2,6,12]. Secondly, THz spectroscopic analysis is based on the signal normalization from free-path or highly reflecting surfaces, and this causes a well-known limitation in the phase value's accuracy and, therefore, in the spectrum retrieval. Inherently, the presence of tilting or curvature on the sample surface makes it difficult to extract accurate values of the complex refractive index [13]. Finally, various additional secondary effects can complicate the analysis of the THz data, such as Fabry–Perot, multiple-scattering, and water vapor in the atmosphere, which pose significant challenges in data pre-processing, particularly when examining heritage artefacts with multiple material layers and uneven surfaces [4,14].

In the past 20 years, researchers have been investigating the potential of THz radiation for examining works of art, ranging from oil paintings on canvas to mummies and architectural specimens. One of the earliest applications of THz imaging dates to 2008, when Jackson et al. showed the capability of this technique to uncover graphite underdrawings beneath a lime plaster layer on a mock-up wall painting sample [14]. In 2010, Fukunaga et al. applied THz imaging to analyze historical mural paintings, comparing the intensity in reflection at far-infrared frequencies with the distribution of pigments determined via Raman and X-ray fluorescence [3]. Since then, THz imaging has expanded to include the examination of wall painting structure, condition, and hidden depictions [5,15–18]. In 2015, Koch-Dandolo et al. applied THz-TD imaging to an easel painting, investigating its stratigraphy for a suspected hidden portrait vaguely emerged from X-ray radiography [19]. By employing recursive signal windowing and threshold clipping, the authors clearly isolated the hidden portrait with a good image contrast [19]. A year later, A. M. Gomez-Sepulveda et al. utilized THz imaging technology on a Mexican work of art to identify concealed paintings beneath the surface and uncover the painting's history. The researchers used a combination of visible, infrared, X-ray, and THz-TD imaging techniques to conduct a comprehensive analysis of the paintings. THz-TD imaging enabled the identification of three layers at different depths, which correspond to their chronological stratification. This technique also revealed an inscription hidden beneath the current composition, attributing the middle layer to Jose Maria Torrez, thus highlighting its benefits for authentication purposes [20].

In all these research studies, THz-TD imaging has been applied to obtain virtual cross-sections of inner layers and to uncover signs of previous conservation treatments. While the research conducted so far has thus mainly explored the THz technique in the time-domain, studies on mapping spectral signatures that implicitly tackle the limitations imposed by real art objects have been less frequent. In fact, data obtained by Fourier-transforming THz-TD from a raster-scanned surface constitutes a 3-dimensional hyperspectral cube, where each spectral image is corrupted by blur and noise to an extent that depends on the frequency itself, a consequence of the broad-band nature of the source. The removal of the joint blur and noise issues was proposed only recently by M. Ljubenovic and collaborators [12]. The authors proposed an approach specifically tailored for broad-band THz-TDI, starting

from image restoration methods commonly applied to remote hyperspectral imaging at visible and near-infrared frequencies. The methodology was extended to the acquisition in reflection geometry for opaque objects and demonstrated to effectively cancel the effects of beam shape and reduce noise between 0.25 and 6 THz [4,12]. The second problematic condition when dealing with heritage object, i.e., studying uneven surfaces, was tackled by A. Artesani and co-authors in 2023 [13]. They proposed a self-referenced method to computationally remove surface geometrical curvature and consequently correct the phase value, enabling the determination of more accurate material absorption coefficients [14,21].

In order to exploit the methods developed so far for THz-TD imaging and spectroscopy, a mock-up sample that mimics an ancient fresco painting was created. The purpose of this mock-up was to illustrate the step-by-step process followed to determine the absorption coefficient value in a pixel-wise characterization and compare the results with point-like measurements performed on mineral pigment pellets [21]. The pros and cons of the data processing and the strategy used to avoid inaccurate results and determine the spectral signature of the painted surface are presented and critically discussed.

2. Materials and Methods

2.1. Materials

Data obtained in this study were collected from a fresco mock-up, which was prepared mimicking an ancient Roman fresco [22–24]. The first preparatory layer (*arriccio*) is composed of fluvial sand as an inert material and slaked lime as a binder, in a 3:1 ratio. The second layer (*intonachino*), which contains the painted layers, is composed of marble powder as an inert material and slaked lime as a binder (1:1). On the top of the two preparatory lime plasters, a homogeneous paint layer was created with respect to the fresco technique: the powder pigment minium was suspended in water and carbonated into the *intonachino*. At a later stage, *a secco* retouches were made by dispersing powder pigments (i.e., Egyptian blue, azurite, and cinnabar) in slaked lime water. The pattern of the drawing and a picture of the mock-up are shown in Figure 1. Pictures of the fresco mock-up profile and cross-section are reported in the Supplementary Materials (SM), Figure S1.

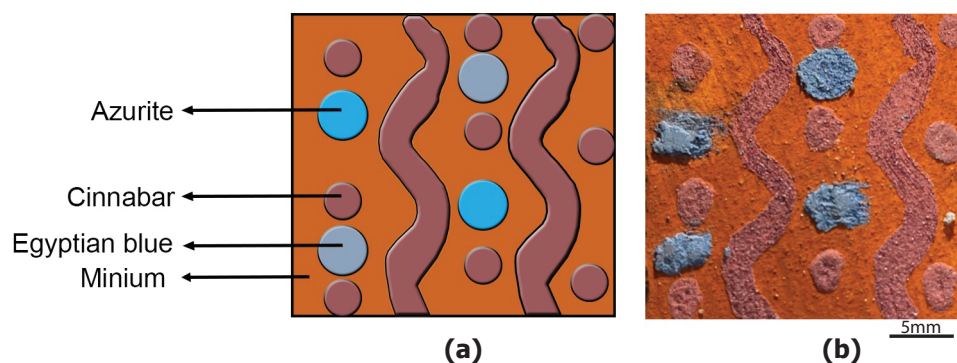


Figure 1. (a) Schematic illustration and (b) optical picture of the mock-up sample.

2.2. Methods

The instrument utilized in this research is a commercial THz-TD system (TOPTICA Photonics, Munich, Germany, TeraFlash Pro), equipped with a mode-locking Erbium-doped fiber laser ($\lambda = 1560 \pm 10$ nm, pulse width 50–60 fs, repetition rate 100 MHz). A thorough description of the system is presented in our previously published papers [13,14,21]. For the purposes of this study, imaging data were acquired using a reflection configuration under a nitrogen atmosphere to suppress air moisture contribution and enhance the spectral identification of pigments. To this scope, the THz-head and the sample holder were placed inside a chamber, with a gas inlet providing continuously flowing N_2 gas. The atmosphere inside the chamber was left stabilizing until steady-state conditions were reached, as determined by monitoring the abatement of air moisture absorption peaks on the real-time

acquired THz spectrum. Once the stable atmosphere was reached, an area of $25 \times 25 \text{ mm}^2$ on the mock-up was raster-scanned with a step-size of 0.2 mm; each point averaged 7 acquisitions. Back-reflected signals were collected in a temporal window of 70 ps (time step of 0.05 ps) that implies a frequency resolution of approximately 13 GHz.

Here, the procedures developed in the previous works have been combined to extract both temporal and spectral details from the time and frequency domains, respectively. Firstly, surface geometrical distortion was removed in time domain using the self-referenced method, as described in detail in [21]. In summary, this method involves computationally removing the temporal drift induced by the axial misalignment, after a surface curvature interpolation. The self-referenced method allows for the removal of object geometrical curvature without imposing any experimental constraints and can be applied regardless of the acquisition system used, as it relies only on post-processing signal analysis. The results are presented in terms of time-of-flight (ToF) maps of the surface structure, and the spatial surface thicknesses are determined using the simple conversion:

$$\Delta h = \frac{c}{2n_0} \frac{\Delta t}{\cos \theta} \quad (1)$$

where $c = 0.02998 \text{ mm/ps}$ is the speed of light, Δt is the temporal difference between two levels, n_0 is the refractive index, and θ is the incident angle of the radiation. For the sake of simplicity, we assumed here that the refractive index is equal to the unit and the radiation has a normal incidence.

The amplitude and the phase of the complex electric field $E_s(\omega)$ were then determined via Fourier transforming time domain spectra and normalized to the reference signal $E_{ref}(\omega)$, which was obtained by averaging the signals from an area of $3 \times 3 \text{ mm}$ on a metallic mirror (Eksma Optics, Vilnius, Lithuania, 092-0030) in the same experimental condition employed for the mock-up sample. The resulting transfer function \mathcal{H} is given by:

$$\mathcal{H}(\omega) = \frac{E_s(\omega)}{E_{ref}(\omega)} = A(\omega)e^{i\phi(\omega)}. \quad (2)$$

Because of the surface curvature, the phase $\phi(\omega)$ is modified by an additive contribution that linearly increases with axial misalignment and depends on frequency, whereas amplitude variation is much more complex in regard to its non-linear frequency dependence and to intensity beam variation along the axial direction. In the Supplementary Materials (SM) of this work, the experimental evaluation of the consequences of spatial misalignment by measuring the reflected signal from a highly reflective surface, i.e., the metallic mirror, is included to show that such an intensity variation can be neglected if the misalignments are relatively small [4].

The corrected values of the phase $\phi(\omega)$ and amplitude $A(\omega)$ were used to calculate the absorption coefficient $\alpha(\omega)$ of the paint materials using the following equation:

$$\alpha(\omega) = \frac{2\omega}{c} \frac{2\phi(\omega)}{(1 - |A(\omega)|)^2 + \phi^2(\omega)} \quad (3)$$

As performed in a previous work for the analysis on pellet samples [21], spectroscopic maps were determined by considering the integral of $\alpha(\omega)$ over a certain frequency range $\Delta\omega$ for each pixel, without any further corrections.

Finally, given the multi-layer structure of the sample, an investigation of its stratigraphy was included. To achieve this, temporal deconvolution was applied to time-domain data to separate the contribution from underlying layers that were otherwise undetectable in the original time profile. In general, the THz back-reflected signal is the convolution of the incident THz signal and the impulse response function (IRF). The IRF represents the pure reflected signal if the incident signal were an infinitesimal impulse in time. To obtain the IRF, we employed the method described in [25,26] and calculated the inverse

Fourier transform of the ratio of the reflected and incident signals, the latter in the form of a reference signal:

$$IRF(t) = FFT^{-1} \left[\frac{E_s(\omega)}{E_{ref}(\omega)} \right] \quad (4)$$

In this way, the number of interfaces in the sample and their topography were retrieved by calculating the maximum intensity projection of the signal over certain time frames.

3. Results and Discussion

The first issue to tackle when considering THz-TD back-reflection spectroscopy on a painted object is the surface shape of the sample. The surface geometry of ancient frescoes, for instance, is shaped by the irregularities of the wall and lime plaster underneath. Time domain spectroscopy is inherently affected by these characteristics of the object, as axial misalignment causes a variation of the amplitude and phase of the electric field. Therefore, prior to any spectroscopic analysis, the correction for geometrical distortion must be applied. In this section, the following experimental steps were applied: removal of geometrical distortion of the surfaces, determination of the ToF map of the sample, and calculation of the absorption coefficient in the frequency domain for material identification. This protocol enables the calculation of the spectrum in the far-infrared region associated with the material composition.

3.1. Correction of Geometrical Distortions

The surface of the mock-up sample has several reliefs associated with the paint layers, superimposed to a surface curvature generated by the mortar and lime plaster substrate. Figure 2a shows the ToF map of the back-reflected signal from raw data. The maximum variation of ToF is about 5 ps, which corresponds to almost 800 μm . The first step of the self-referenced method for geometrical distortion removal consists of determining the surface shape described as a function of the two spatial dimensions. The determination of the object shape (as defined in [13]) is not always straightforward. It might be that the surface cannot be properly approximated with a polynomial curve, which can represent a limitation for the surface distortion correction. In our case, we could interpolate the surface of the mock-up sample with a second- and third-order polynomial function along the x and y directions, respectively, obtaining an adjusted- R^2 value of 0.896. The result is shown in Figure 2b. The modelled object shape does not take into account the local geometries, such as local roughness and reliefs generated by the paint layers. This enables us to maintain the overall topography of the surface while removing the unwanted curvature.

The temporal shift of the raw data obtained from the THz back-reflected signal led to the result shown in Figure 2c, whereas the profile of the corrected surface in spatial dimensions is illustrated in Figure 2d. The new dataset does not differ from the original THz signal, apart from a zero-padding used to shift the temporal peak position. This zero-padding does not affect the spectroscopic characteristic of the THz signal but has the consequence of restoring the surface flatness. In the specific case of the mock-up sample, the conversion from temporal to spatial profile showed that the corrected object surface delineates an almost flat region, shaped by a roughness of 100 μm in height. On top of it, the *a secco* retouches have thicknesses between 100 μm and 200 μm , while three painted spots have higher thicknesses that reach 300 μm and 400 μm .

This pre-processing step is fundamental before proceeding into the analysis of material spectra in the frequency domain, as the surface curvature correction reduces the error induced in the phase. The effects of surface geometrical distortions and curvature correction on the amplitude are limited to a reduction of intensity, which remains below 5% with respect to the focus position if the misalignment is less than 5 ps, as in this work (see SM, Figures S2 and S3).

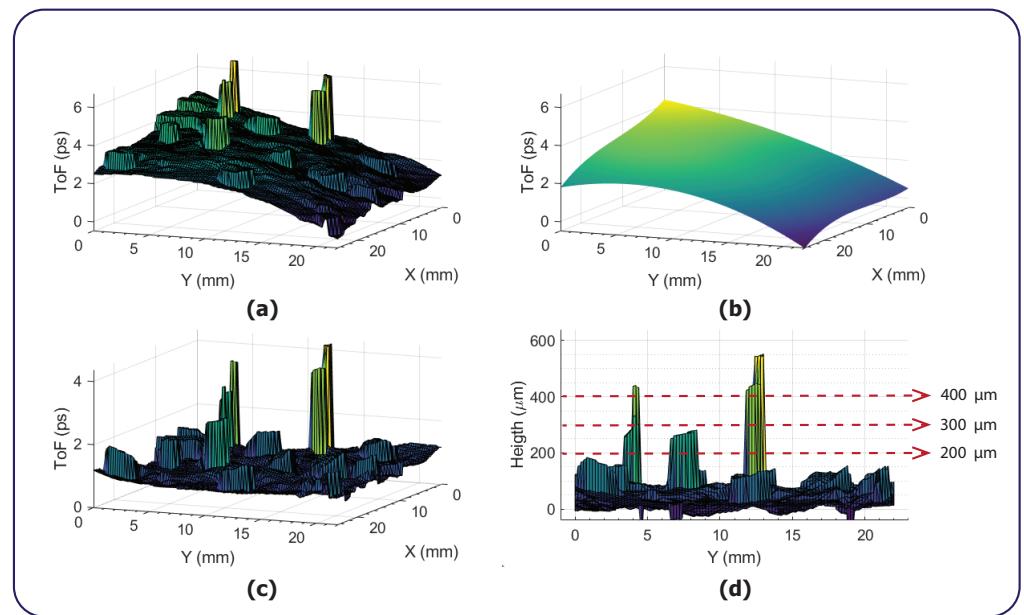


Figure 2. Temporal profile of the sample before and after curvature removal. (a) Original ToF map of the sample. (b) Approximated ToF curve found from fitting the original object surface with a polynomial curve. In this case, $f(x,y) = a_1 + a_2x + a_3x^2 + a_4x^3 + a_5y + a_6y^2$, adj. $R^2 = 0.896$. (c) ToF map of the surface object after surface curvature correction. (d) Spatial profile of the thicknesses of the mock-up sample, assuming the refractive index as unit and normal incidence of the THz beam.

3.2. Absorption Coefficient Maps

After correcting for surface curvature, Fourier transform of the data in the temporal domain was calculated to obtain information on the spectral signature in the frequency domain. In contrast to previously published work conducted on pellets of pure pigment powder, in the present investigation, we dealt with a thin paint layer created using pigments dispersed in water as in the *fresco* technique. This generates an issue related to the amount of material that causes the back-reflection of the signal and introduces secondary effects (such as Fabry–Perot effects) between two consecutive layers. The extension of these limitations was therefore considered.

The value of the absorption coefficient $\alpha(\omega)$ was calculated in the frequencies ranging between 50 and 120 cm^{-1} , chosen on the basis of the performance of the adopted instrument. Figure 3a represents the distribution of the absorption coefficient over the entire surface, integrated between 50 and 120 cm^{-1} . The intensity of $\alpha(\omega)$ is determined by the specific absorption properties of the material and the topography of the surface. In greyscale, Figure 3b shows that the darker pixels correspond to less reflective materials with respect to the background. Four regions of interest (ROIs) composed by different material composition and number of painted layers were selected. The ROI-A corresponds to cinnabar, which can be considered as reflective as the ROI-B, the minium and first layer of the entire mock-up surface. Different reflective intensities are instead obtained from Egyptian blue (ROI-C) and azurite (ROI-D), which are associated with darker areas.

Figure 3c shows the average THz-TD signal obtained from each of the selected ROIs. In the same plots, the standard deviation is represented to report the signal variation among each point of the area. First and foremost, there are important differences to underline. The most reflective materials, corresponding to ROI-A and B, have a single and sharp THz peak, usually associated with single back reflection. If there is a contribution from layers underneath, it is negligible. Moreover, the peak distribution over the entire area is highly homogeneous, yielding small standard deviation values. Different results are obtained for ROI-C and D, which are less reflective at THz frequencies. The average THz signal from ROI-C shows a spread signal without any defined peak, possibly caused by

the superposition of two back-reflected signals generated by a thin layer on top of another reflective layer. In this case, we could not separate the two contributions and advance any hypothesis on the composition of the material. In the last example, the ROI-D shows two broad but separated THz signals, although they are still too close and weak to exclude one from the another with a signal filtering process. It turns out that the presence of multiple layers and weakly reflective materials might highly complicate the spectral analysis of a painted surface, even if one can properly calculate the absorption coefficient for each point of the sample surface. For this reason, we suggest considering the temporal signal before any spectroscopic analysis.

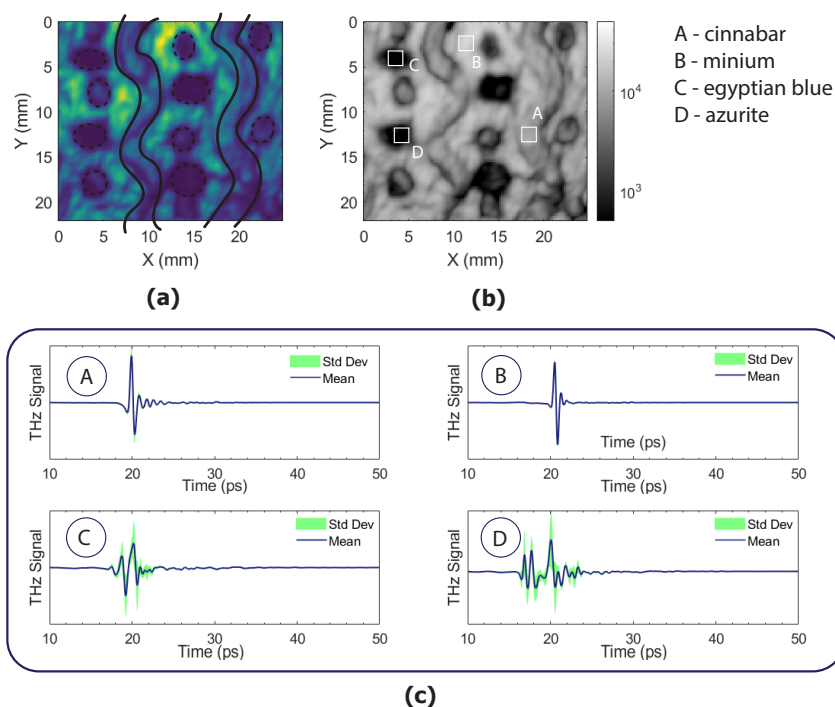


Figure 3. (a) Absorption coefficient map integrated between 50 and 120 cm^{-1} ; region of interest (ROIs) associated with different paint compositions are segmented. (b) Absorption coefficient intensity in grey-scale color, evidencing the region with higher (white) and lower (black) reflectivity in the far infrared region. On the same map, ROIs with different material composition and number of layers are reported. (c) Mean and standard deviation of the THz signal in the four ROIs.

The absorption coefficient spectra of the strong reflective ROIs were compared with the spectra obtained from pure pellet samples (as shown previously [21]). Figure 4 illustrates the spectra obtained from ROI-A and B, which correspond to cinnabar and minium, two red pigments, respectively. Cinnabar (HgS) exhibits A_2 and E lattice vibrations in the THz region, with absorption peaks at 39.0, 41.4, and 88.0 cm^{-1} . On the mock-up sample, the first two peaks around 40 cm^{-1} , which are the most intense (Figure 4a), were clearly identified. Their peaks position greatly corresponds to those detected in the pellet sample in the previous work. Similarly, in the far-infrared region, the absorption peaks of minium (Pb_3O_4), as depicted in Figure 4b, were detected. This pigment has an intense peak at the signals 65.4 cm^{-1} and a small peak at 57.0 cm^{-1} , both due to translations of O and Pb atoms along the crystallographic b-axis. A peak at 74.5 cm^{-1} was also detected and assigned to translation along the c-axis, while another less intense absorption peak at 84 cm^{-1} , with no assignment, was found. However, multiple reflections prevented us from detecting any spectroscopic signals that were expected from the analysis of the pure pigment, as the superimposed back-reflected signals from two layers in time-domain were not sufficiently far apart to apply filtering or other signal separation procedures and thus retrieve their individual contributions.

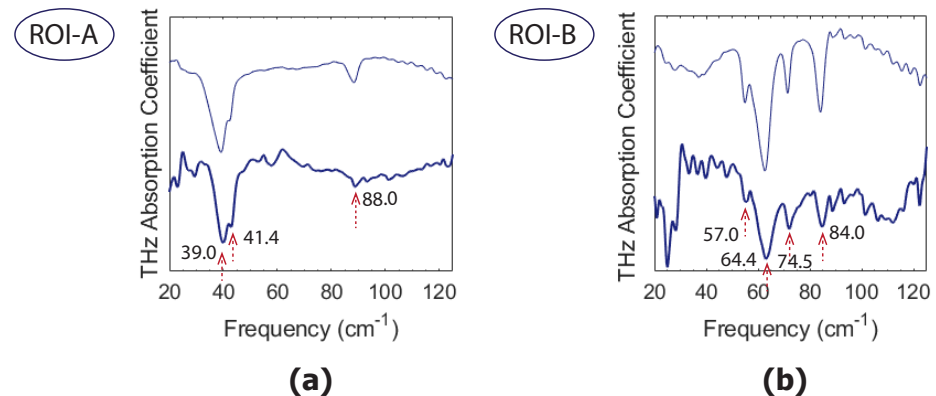


Figure 4. (a) Absorption coefficient spectrum of ROI-A (cinnabar, HgS). The arrows indicate the absorption coefficient peak of cinnabar at 39.0, 41.4 and 88 cm^{-1} . (b) Absorption coefficient spectrum of ROI-B (minium, Pb_3O_4). The arrows indicate the absorption coefficient peak of minium at 57.0, 64.4, 74.5 and 84 cm^{-1} .

3.3. Temporal Deconvolution

As discussed in the previous sections, the THz-TD signals should be characterized by peaks corresponding to the interfaces included in the material stratigraphy. While the first peak is usually well defined, as it is much more intense, the reflection from layers underneath is less appreciable, especially when there is high signal absorption and scattering and small thicknesses. In the case of the sample considered here, we showed that, depending on the material composition, the back-reflected signals are characterized by a well-shaped peak corresponding to the first interface, or by multiple superimposed peaks if the first layer is not thick or absorbing enough. Even less information can be retrieved from the inner structure, as the signal-to-noise ratio drops at higher temporal shift.

To retrieve the impulse response function (IRF) of the THz signal, and thus remove the contribution of the temporal profile of the exciting pulse, temporal deconvolution on the uncorrected data was employed. The resulting B-scan profile of the IRF is showed in Figure 5b. In detail, the figure shows the IRF across the line $x = 11.8$ mm, after imposing a lower thresholding to the intensity signal to exclude noise fluctuations and better enhance peaks position. The threshold used was determined by calculating the mean and standard deviation of the IRF over the entire profile, with the threshold value corresponding to the mean plus two times the standard deviation. In this way, a difference of at least 2σ between the average noise and IRF peaks was ensured.

An example of the IRF profile at one point of the raster-scanned surface is provided in Figure 5a. The IRF shows four peaks, conceivably corresponding to different interfaces. The peaks are consistently found in every IRF profile along the selected line, as illustrated by the B-scan map. An inset is provided for a better description of the first and third peaks, which lie around 3 ps and 30 ps, respectively. As depicted on the right side of Figure 5b, the first layer is not flat and has a rough shape, while the inner peaks delineate a different and more linear profile. The first peak is associated with the air–paint interface, the second (weak) peak could be associated with the interface between the painted layer and the *intonachino*. In fact, according to the fresco painting tradition, the *intonachino* was not completely dried at the time the paint layer is applied, and thus pigment particles are incorporated in the underlying layer. The third peak could thus be associated with the interface between *intonachino* and *arriccio*. It is worth noting that the temporal distances between the detected interfaces correspond to the optical thicknesses of the layers and differ from the physical thicknesses, depending on the refractive index of the material. Therefore, IRF peaks with higher distances does not necessarily correspond to a higher thickness of the layer.

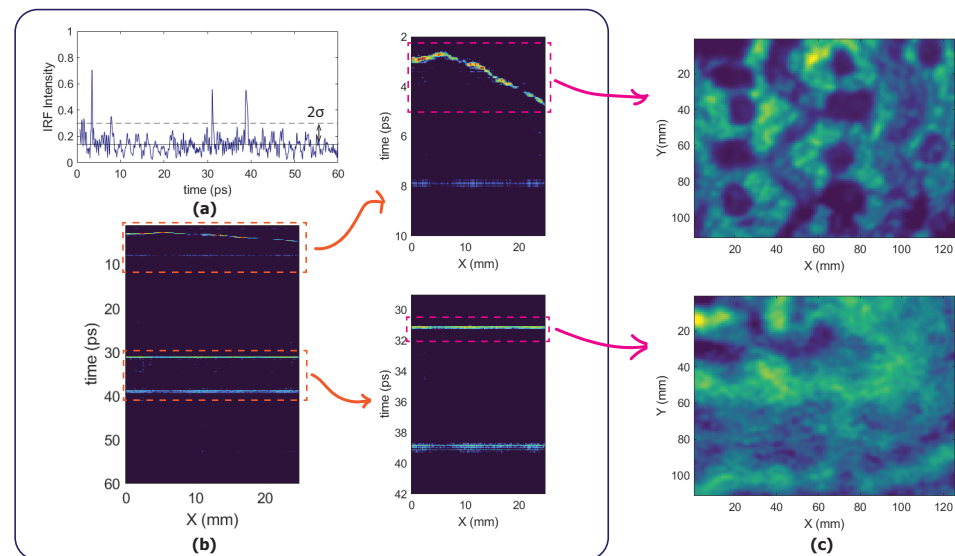


Figure 5. Results of the temporal deconvolution employed on the uncorrected data. (a) Impulse Response Function (IRF) across the line $x = 11.8$ mm and $y = 5$ mm. The horizontal black line is the average value of the IRF and the dotted lines represent the $\pm 2\sigma$ (standard deviation) range. (b) B-scan of the IRF across the line $x = 11.8$ mm, and two details of the first layer (top) and third layer (bottom). (c) Maximum intensity projection of the IRF of the first layer (top) and second layer (bottom) that identify their topography.

The maximum intensity projection to retrieve the topography of the inner surface was also performed. First, we calculated the maximum intensity projection on the outer surface to ensure that the detected surface is associated with the first layer. As illustrated in Figure 5c on top, the image of the first surface is confirmed to be that of the paint layers. The maximum intensity projection of the inner surface instead presents a more irregular geometry (Figure 5c, bottom), not showing any specific structure but overall shaped by hills and valleys, as could be associated with a mortar base. Nevertheless, the proper identification of the layers could be confirmed only by cross-section of the painted stratigraphy.

4. Conclusions

While THz imaging has primarily been applied for studying virtual cross-sections of painted artworks or determining the spectral signature in the far-infrared frequencies from point-like measurements, the simultaneous integration of imaging and spectroscopic mapping has never been proposed before due to inherent limitations in processing THz signals. In this study, a laboratory-designed approach that combines imaging acquisition and spectroscopic analysis was proposed to explore the potential advantages and limitations of THz-TD on real artworks. To achieve this, we addressed issues related to axial misalignments and electric field drift, and subsequently determined the absorption coefficient map between 20 and 120 cm^{-1} .

In the specific case of the sample investigated here, the presence of a non-flat surface—with approximately 800 μm of height difference between the lower and upper parts—could have potentially resulted in an inaccurate determination of phase values, making it impossible to calculate the frequency-dependent absorption coefficient. Nevertheless, we have successfully demonstrated that, by removing this unwanted curvature, an accurate correction of the phase signal and the surface topography was successfully achieved. This crucial correction has enabled us to obtain more precise absorption coefficient values and retrieve real spectroscopic signatures from painted materials when they exhibit absorption in the THz region of frequencies. In general, THz-TD can identify and discriminate metal

oxides in a contactless and non-ionizing manner, ensuring a safer analysis of cultural heritage surfaces.

However, a potential limitation in the relatively low reflecting power of certain painting materials must be considered. Particularly, the presence of thin layers of paint composed of Egyptian blue and azurite, alongside highly reflective pigments, presented challenges for the system in accurately detecting their spectra. It is important to take this aspect into consideration for future studies involving real artwork.

Virtual cross-section imaging remains one of the significant advantages of THz-TD. Temporal deconvolution enables the detection of inner interfaces and the visualization of internal layer shapes. This method proves particularly advantageous when investigating suspicious pre-treatments and when a high-resolution imaging device with millimeter depth of field is required.

Undoubtedly, the utilization of far-infrared electromagnetic radiation offers significant advantages. The integration of THz-TD and the different working modality of THz-TD (i.e., imaging and spectroscopy) further advances the capabilities of this technique, making it highly beneficial for routine analysis of cultural heritage.

Supplementary Materials: The following supporting information can be downloaded at: <https://www.mdpi.com/article/10.3390/heritage6070276/s1>, Figure S1: Sample Cross-Sections; Figure S2: THz-TD profile at different axial positions; Figure S3: Amplitude intensity at different axial positions before and after surface distortion correction.

Author Contributions: Methodology, A.A.; Formal analysis, A.A.; Investigation, F.A. and R.L.; resources, A.T.; writing—original draft preparation, A.A., F.A. and R.L.; writing—review and editing, A.A., F.M., M.A.B. and A.T.; supervision, A.T. All authors have read and agreed to the published version of the manuscript.

Funding: This research received no external funding.

Data Availability Statement: Data available on request due to restrictions.

Acknowledgments: The authors would like to express their gratitude to prof. Stefano Bonetti (Ca' Foscari University of Venice) for providing access to the THz instrument and for his support throughout their research on this domain.

Conflicts of Interest: The authors declare no conflict of interest.

References

1. Fukunaga, K. *THz Technology Applied to Cultural Heritage*; The Hong Kong University of Science and Technology: Hong Kong, China, 2012; ISBN 9781467315975.
2. Catapano, I.; Soldovieri, F. *THz Imaging and Data Processing: State of the Art and Perspective*; Elsevier Inc.: Amsterdam, The Netherlands, 2018; ISBN 9780128124291.
3. Fukunaga, K.; Hosako, I.; Kohdzuma, Y.; Koezuka, T.; Ikari, T.; Du, X. Terahertz analysis of an east asian historical mural painting. *J. Eur. Opt. Soc. Rapid Publ.* **2010**, *5*, 10024. [[CrossRef](#)]
4. Ljubenic, M.; Artesani, A.; Bonetti, S.; Traviglia, A. Beam-Shape Effects and Noise Removal from THz Time-Domain Images in Reflection Geometry in the 0.25–6 THz Range. *IEEE Trans. Terahertz Sci. Technol.* **2022**, *12*, 574–586. [[CrossRef](#)]
5. Krügener, K.; Ornik, J.; Schneider, L.M.; Jäckel, A.; Koch-dandolo, C.L.; Castro-camus, E.; Riedl-siedow, N.; Koch, M.; Viöl, W. Terahertz Inspection of Buildings and Architectural Art. *Appl. Sci.* **2020**, *10*, 5166. [[CrossRef](#)]
6. Fukunaga, K.; Picollo, M.; Fukunaga, K.; Picollo, M. Terahertz Spectroscopy Applied to the Analysis of Artists' Materials. *Appl. Phys. A* **2010**, *100*, 591–597. [[CrossRef](#)]
7. Picollo, M.; Fukunaga, K.; Labaune, J. Obtaining Noninvasive Stratigraphic Details of Panel Paintings Using Terahertz Time Domain Spectroscopy Imaging System. *J. Cult. Herit.* **2015**, *16*, 73–80. [[CrossRef](#)]
8. Fukunaga, K.; Ogawa, Y.; Hayashi, S.; Hosako, I. Terahertz Spectroscopy for Art Conservation. *IEICE Electron. Express* **2007**, *4*, 258–263. [[CrossRef](#)]
9. Tzortzakos, J.M.S. Nonlinear Imaging and THz Diagnostic Tools in the Service of Cultural Heritage. *Appl. Phys. A* **2012**, *106*, 257–263. [[CrossRef](#)]
10. Lee, J.E.; Lee, H.; Kim, J.; Jung, T.S.; Kim, J.H.; Kim, J.; Baek, N.Y.; Song, Y.N.; Lee, H.H.; Kim, J.H. Terahertz Spectroscopic Analysis of the Vermilion Pigment in Free-Standing and Polyethylene-Mixed Forms. *ACS Omega* **2021**, *6*, 13802–13806. [[CrossRef](#)]
11. Banks, P.A.; Kleist, E.M.; Ruggiero, M.T. Investigating the Function and Design of Molecular Materials through Terahertz Vibrational Spectroscopy. *Nat. Rev. Chem.* **2023**, *7*, 480–495. [[CrossRef](#)]

12. Ljubenovic, M.; Zhuang, L.; De Beenhouwer, J.; Sijbers, J. Joint Deblurring and Denoising of THz Time-Domain Images. *IEEE Access* **2021**, *9*, 162–176. [[CrossRef](#)]
13. Artesani, A.; Ljubenovic, M.; Traviglia, A.; Bonetti, S. Self-Referenced Method for Geometrical Distortion Removal in THz Time-Domain Reflection Imaging. *IEEE Trans. Terahertz Sci. Technol.* **2023**, *13*, 113–121. [[CrossRef](#)]
14. Artesani, A.; Ljubenovic, M.; Bonetti, S.; Traviglia, A. Processing and Analysis of THz Time-Domain Spectroscopy Imaging Applied to Cultural Heritage. In *Optics for Arts, Architecture, and Archaeology VIII*; SPIE: Bellingham, DC, USA, 2021; Volume 11784, p. 12. [[CrossRef](#)]
15. Jackson, J.B.; Mourou, M.; Whitaker, J.F.; Duling, I.N.; Williamson, S.L.; Menu, M.; Mourou, G.A. Terahertz Imaging for Non-Destructive Evaluation of Mural Paintings. *Opt. Commun.* **2008**, *281*, 527–532. [[CrossRef](#)]
16. Fukunaga, K. Nondestructive Evaluation of Lined Paintings by THz Pulsed Time-Domain Imaging. *Heritage* **2023**, *6*, 3448–3460. [[CrossRef](#)]
17. Seco-Martorell, C.; López-Domínguez, V.; Arauz-Garofalo, G.; Redo-Sanchez, A.; Palacios, J.; Tejada, J. Goya’s Artwork Imaging with Terahertz Waves. *Opt. Express* **2013**, *21*, 17800. [[CrossRef](#)] [[PubMed](#)]
18. Dong, J.; Ribeiro, A.; Vacheret, A.; Locquet, A.; Citrin, D.S. Revealing Inscriptions Obscured by Time on an Early-Modern Lead Funerary Cross Using Terahertz Multispectral Imaging. *Sci. Rep.* **2022**, *12*, 3429. [[CrossRef](#)]
19. Koch-Dandolo, C.L.; Filtenborg, T.; Fukunaga, K.; Skou-Hansen, J.; Jepsen, P.U. Reflection Terahertz Time-Domain Imaging for Analysis of an 18th Century Neoclassical Easel Painting. *Appl. Opt.* **2015**, *54*, 5123–5129. [[CrossRef](#)]
20. Gomez-Sepulveda, A.M.; Hernandez-Serrano, A.I.; Radpour, R.; Koch-Dandolo, C.L.; Rojas-Landeros, S.C.; Ascencio-Rojas, L.F.; Zarate, A.; Hernandez, G.; Gonzalez-Tirado, R.C.; Insaurralde-Caballero, M.; et al. History of Mexican Easel Paintings from an Altarpiece Revealed by Non-Invasive Terahertz Time-Domain Imaging. *J. Infrared Millim. Terahertz Waves* **2017**, *38*, 403–412. [[CrossRef](#)]
21. Artesani, A.; Lamuraglia, R.; Menegazzo, F.; Bonetti, S.; Traviglia, A. Terahertz Time-Domain Spectroscopy in Reflection Configuration for Inorganic and Mineral Pigment Identification. *Appl. Spectrosc.* **2023**, *77*, 74–87. [[CrossRef](#)] [[PubMed](#)]
22. Mora, P.; Mora, L.; Philippot, P. *La Conservazione Delle Pitture Murali*; Compositori: Bologna, Italy, 2003; ISBN 8877942797.
23. Rowland, I.D.; Howe, T.N. *Vitruvius: ‘Ten Books on Architecture’*; Cambridge University Press: Cambridge, UK, 2001.
24. Izzo, F.; Arizzi, A.; Cappelletti, P.; Cultrone, G.; De Bonis, A.; Germinario, C.; Graziano, S.F.; Grifa, C.; Guarino, V.; Mercurio, M.; et al. The Art of Building in the Roman Period (89 B.C.–79 A.D.): Mortars, Plasters and Mosaic Floors from Ancient Stabiae (Naples, Italy). *Constr. Build. Mater.* **2016**, *117*, 129–143. [[CrossRef](#)]
25. Walker, G.C.; Bowen, J.W.; Labaune, J.; Jackson, J.-B.; Hadjiloucas, S.; Roberts, J.; Mourou, G.; Menu, M. Terahertz Deconvolution. *Opt. Express* **2012**, *20*, 27230–27241. [[CrossRef](#)]
26. Koch Dandolo, C.L.; Lopez, M.; Fukunaga, K.; Ueno, Y.; Pillay, R.; Giovannacci, D.; Le Du, Y.; Bai, X.; Menu, M.; Detalle, V. Toward a Multimodal Fusion of Layered Cultural Object Images: Complementarity of Optical Coherence Tomography and Terahertz Time-Domain Imaging in the Heritage Field. *Appl. Opt.* **2019**, *58*, 1281–1290. [[CrossRef](#)] [[PubMed](#)]

Disclaimer/Publisher’s Note: The statements, opinions and data contained in all publications are solely those of the individual author(s) and contributor(s) and not of MDPI and/or the editor(s). MDPI and/or the editor(s) disclaim responsibility for any injury to people or property resulting from any ideas, methods, instructions or products referred to in the content.